Applied Physics Letters ARTICLE pubs.aip.org/aip/apl

Ultra-broadband low-frequency high-efficiency acoustic energy harvesting with metamaterial-enhanced loudspeakers

Cite as: Appl. Phys. Lett. **123**, 073903 (2023); doi: 10.1063/5.0158079
Submitted: 14 May 2023 · Accepted: 30 July 2023 ·
Published Online: 16 August 2023

Xiuyuan Peng, Junfei Li, and Steven A. Cummer[a)]

AFFILIATIONS

Department of Electrical and Computer Engineering, Duke University, Durham, North Carolina 27708, USA

Note: This paper is part of the APL Special Collection on Fundamentals and Applications of Metamaterials: Breaking the Limits.
[a)]**Author to whom correspondence should be addressed:** cummer@duke.edu

ABSTRACT

Acoustic energy harvesters (AEHs) open up opportunities to recycle noise waste and generate electricity. They provide potential power solutions to a wide range of sensors. However, the practicality of AEHs has long been limited by their narrow bandwidths and low efficiencies. In this study, we present an ultra-broadband AEH and a highly efficient AEH that transforms sound energy into usable electrical power. Our broadband device comprises an electrodynamic loudspeaker driver and an optimized acoustic metamaterial matching layer and is capable of converting 7.6% to 15.1% of total incident sound energy from 50 to 228 Hz. Moreover, we demonstrate that by replacing the loudspeaker surround with a lower-loss material such as PDMS, the energy conversion rate can be significantly increased to 67%. The proposed broadband AEH has a fractional bandwidth eight times the state-of-the-art, while the proposed highly efficient AEH has a peak efficiency three times the state-of-the-art. The outstanding performance makes our designs cost-effective and scalable solutions for noise reduction and power generation.

Noise pollution is a common issue in our daily lives, and a significant portion of acoustic research focuses on reducing and controlling it. However, noise contains acoustic energy that could be captured and utilized for practical purposes. There is a growing interest in developing acoustic energy harvesters (AEHs)[1] to transform noise waste into electricity. Recent studies have explored various sound-to-electric energy conversion methods such as piezoelectric, electromagnetic, triboelectric, and flexoelectric[1–4] with most existing AEHs relying on a single piezoelectric patch. However, this approach has two major drawbacks. First, the high characteristic acoustic impedance of most piezoelectric materials means most of the sound energy is reflected instead of absorbed at the hard surface. Second, the high Q factor intrinsic to typical piezoelectric units may enhance the energy conversion efficiency at its resonant frequency but also reduces the broadband performance that is crucial in real-world applications. Some AEHs claimed to be broadband using piezoelectric technology may actually have "multiband"[5] performance due to their spiky frequency response curves.[6–9]

The use of electromagnetic transduction offers a promising path for sound energy harvesting. The process involves a thin membrane layer that vibrates in response to sound, causing an attached coil to move within a magnetic field and generate electricity.[10–12] This is how electrodynamic microphones and inverse loudspeakers work.[10] Since the membrane is usually made of lightweight materials, the acoustic coupling can be significantly better than piezoelectric materials when properly designed. The emergence of highly efficient neodymium magnets in recent years also provides better electro-mechanical coupling. Recently, there is a growing trend of using metamaterial impedance matching layers to increase the bandwidth of acoustic devices.[13]

In this paper, we present an approach to sound energy harvesting using an electrodynamic loudspeaker driver and a custom-designed metamaterial impedance matching layer. The low mechanical loss of the vibrating diaphragm ensures high transduction efficiency, while the metamaterial facilitates broadband energy harvesting instead of only at the resonant frequency of the driver. Our ultra-broadband AEH in Fig. 1 has the ability to convert 7.6%–15.1% of incident sound energy into usable electrical power within a fractional bandwidth of 128%. This represents a significant improvement over previous AEHs that typically have fractional bandwidths of 15% or less.[14] Furthermore, by carefully engineering the mechanical loss of the

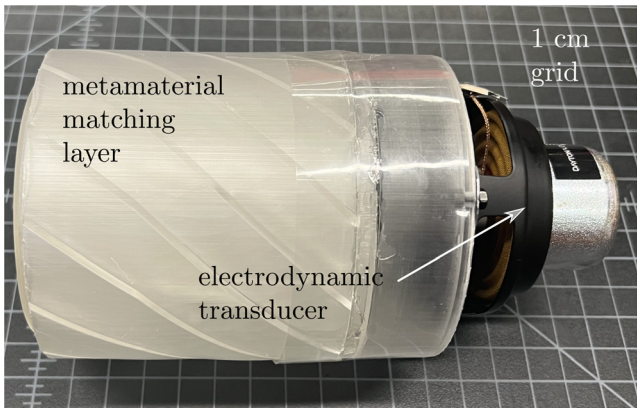

FIG. 1. Broadband AEH with metamaterials.

surround with the custom-made PDMS material, we have achieved a single-frequency energy conversion rate of 67%, which is three times the highest efficiency[10] (23%) previously recorded in the literature. Our AEHs are a great solution in environments with high levels of environmental noise, thanks to their superior energy harvesting efficiency and wider operating bandwidth.

Electrodynamic loudspeakers are the source of many of the artificial sounds we hear today. By leveraging the reciprocity of the electromechanical transduction process, a commercially available loudspeaker unit can be transformed into an acoustic energy harvester (AEH) by immersing it in sound fields and connecting an electrical load to its terminals. This concept is similar to an electric motor, which can also function as a generator by reversing the direction of excitation. Figure 1 shows the proposed broadband AEH, which includes an electrodynamic loudspeaker and a metamaterial impedance matching layer in the front.

To accurately predict the energy harvesting performance of our device, an analytical theory taking into account various parameters is considered. As we are mainly focused low frequencies, where the wavelength is much longer than the size of the AEH, the lumped-element circuit model as is illustrated in Fig. 2 will suffice.

In Fig. 2(a), we present the proposed AEH as an equivalent circuit diagram. The system is comprised of three parts, acoustical, mechanical, and electrical, from left to right. In the acoustical section (left), p_s is the source sound pressure that we aim to reduce, and p_{in} is the incident sound pressure on the loudspeaker diaphragm after it has passed through the transmission line **T**. The mechanical part (middle) and the electrical part (right) primarily consist of Theile-Small parameters[15] of the loudspeaker unit, with the exception of the electrical load resistance R_L and the mechanical compliance of the back cavity $C_{mb} = V_b/\rho_0 c_0^2 S_d^2$, where ρ_0 and c_0 are the air density and sound speed, respectively. u_d represents the diaphragm's vibration velocity, i_e is the current flowing in the loudspeaker coil, V_b is the volume of the back cavity, and S_d is the surface area of the diaphragm.

To simplify the calculation, we reduce Fig. 2(a) to a unified acoustic circuit as shown in Fig. 2(b). Here, Z_{as}, Z_{ab}, and Z_{ae} are the acoustic impedances of the moving cone, back cavity, and coil/load resistor loop, respectively. We have

$$Z_{as} = Z_{ms}/S_d^2 = [R_{ms} + j\omega M_{md} + 1/j\omega C_{ms}]/S_d^2, \quad (1)$$

$$Z_{ab} = Z_{mb}/S_d^2 = 1/j\omega C_{mb} S_d^2, \quad (2)$$

$$Z_{ae} = Z_{me}/S_d^2 = Bl^2/(R_e + j\omega L_e + R_L)S_d^2, \quad (3)$$

where $\omega = 2\pi f$ is the angular frequency. Once the values of all parameters are determined, we can derive the volume velocity of the air moving with the loudspeaker cone

$$U_d = p_{in}/(Z_{as} + Z_{ab} + Z_{ae}), \quad (4)$$

and the velocity of the vibration cone itself

$$u_d = U_d/S_d. \quad (5)$$

With Faraday's law, we get the current flow in the coil

$$i_e = Blu_d/(R_e + j\omega L_e + R_L) \quad (6)$$

and the output power (RMS) of the AEH

$$P_{out} = i_e^2 R_L/2. \quad (7)$$

Meanwhile, the input acoustic power from the source is

$$P_{in} = p_s^2 S_t/2\rho_0 c_0, \quad (8)$$

where S_t is the cross section area of the transmission line. This gives us the power conversion efficiency $\eta = P_{out}/P_{in}$. Also, if we assume the transmission line to be lossless, the sound absorption coefficient α can be calculated by[16]

$$\alpha = 1 - |\Gamma|^2, \quad (9)$$

$$\Gamma = \frac{Z_{a,in} - Z_0}{Z_{a,in} + Z_0}. \quad (10)$$

Here, the input acoustic impedance of the AEH is

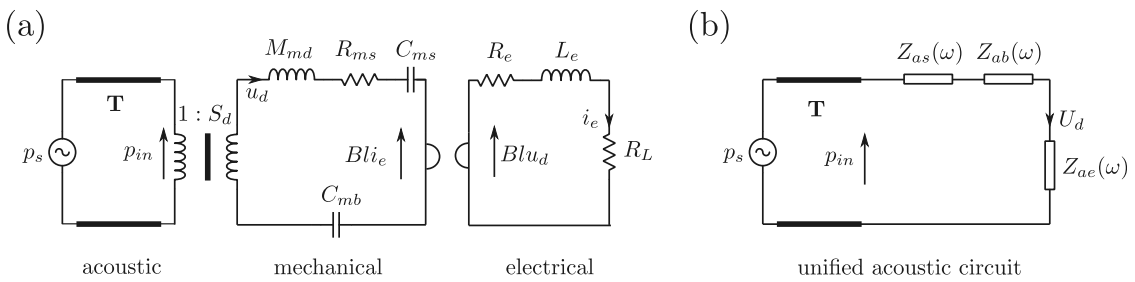

FIG. 2. Equivalent lumped-element circuit of the proposed AEH.

$$Z_{a,in} = Z_{as} + Z_{ab} + Z_{ae}, \tag{11}$$

and the characteristic acoustic impedance of air in the transmission line is

$$Z_0 = \rho_0 c_0 / S_t. \tag{12}$$

Next, the validity of our theoretical model is verified through numerical simulations. We utilize COMSOL Multiphysics 5.6, a software that employs the finite element method (FEM), to generate the corresponding efficiency and sound absorption curves of the loudspeakers. The pressure acoustic module and AC/DC module are coupled in the process with only the lumped element parameters being entered. The software setup follows the sample model provided by the company.[17] Our analytical and numerical results match each other closely, as demonstrated in Fig. 5.

We now develop several design improvements to enhance the bandwidth of the acoustic energy harvester (AEH) to make it more efficient in collecting environmental noise. The design process of most AEHs consists of two parts: first, incident acoustic energy is redirected through a sound concentrator to amplify the amplitude, and then the amplified sound drives the energy converter to produce electricity. For piezoelectric-type AEHs, the operating frequency of the system is determined by the resonant frequency of the sound concentrator,[1,3,4,18–20] which is typically a Helmholtz resonator, a phononic crystal, or a combination of both. It has been shown that it is possible to design a sound concentrator with two or multiple closely positioned resonant peaks that merge to create a wider resonant peak.[21–23] Our loudspeaker-based AEH already has the advantage of a built-in resonant peak due to the oscillating diaphragm, making the sound concentrator redundant for single-frequency operation. However, the same approach can be used by incorporating a more complex transmission line (**T**) in Fig. 2(b) to obtain several resonant features instead of one in the η and α curves, potentially leading to a flatter frequency response curve within the desired frequency band.

While combining multiple resonant peaks in the acoustic circuit is straightforward in theory, its physical implementation is not trivial. Hence, we have chosen to use a parameterized acoustic metamaterial structure as a matching layer between the sound source and the loudspeaker unit and optimize the geometry through a computerized algorithm to produce the best sound energy harvesting performance within the target frequency range.

We aim to measure the properties of the AEH within a cylindrical impedance tube and have selected the spiral unit cell [shown in Figs. 3(a) and 3(b)] as the building block for our metamaterial matching layer. Spiral unit cells introduce phase delay and increased acoustic impedance in the air channels and have been applied for impedance matching previously.[24] The inner and outer radii of the unit cell are denoted by R_{in} and R_{out}, respectively. The length of the unit cell is represented by L, while the spiral angle is denoted by θ_s, and the wall thickness is represented by t_w. To form a spiral segment, we duplicate the spiral unit cell 360° to create a hollow cylinder. This spiral segment has a higher effective refractive index and impedance compared to plain air, which can be approximated using the following equations:

$$n = \frac{1}{\cos\left[\tan^{-1}(3R_{mid}\theta_e/L)\right]}, \tag{13}$$

$$R_{mid} = (R_{in} + R_{out})/2, \tag{14}$$

$$z = \rho_0 c_0 n. \tag{15}$$

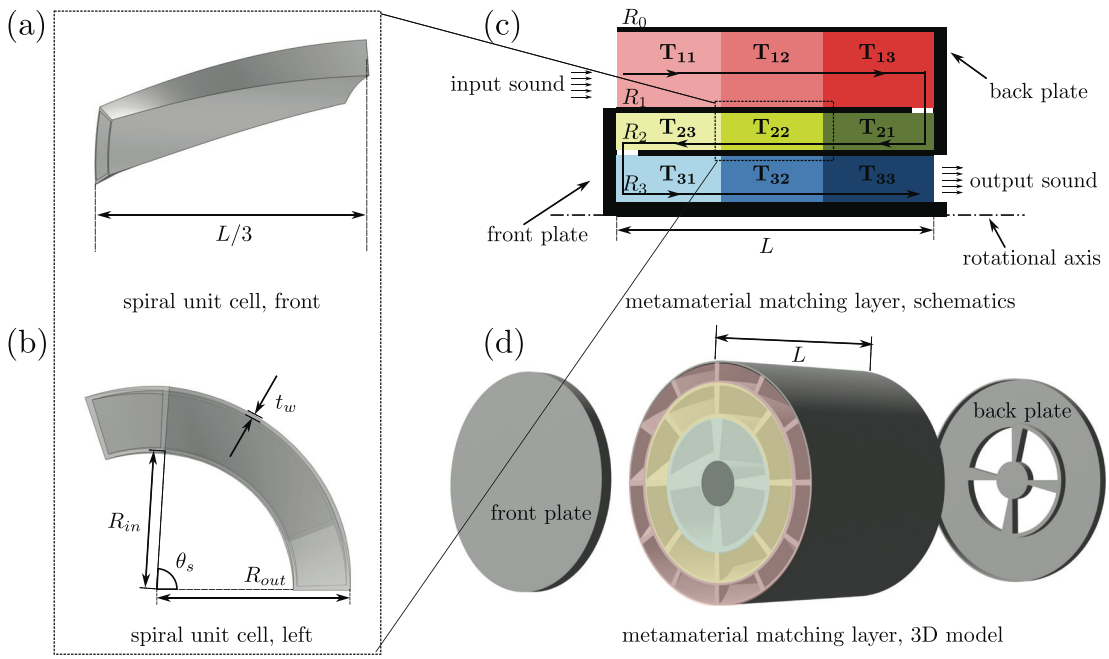

FIG. 3. Metamaterial matching layer with spiral unit cells. (a) Front view of the spiral unit cell. (b) Left view of the spiral unit cell. (c) Schematic view of the metamaterial matching layer. (d) 3D rendering of the metamaterial matching layer.

By changing the spiral angle θ_s, we can tune the phase delay. Thus, we can create multiple internal reflections in the transmission line by linking spiral segments with different characteristic sound speeds and impedances. To make optimal use of the space, we stack three spiral segments to form a spiral channel, and then fold three spiral channels into one cylindrical metamaterial matching layer, with the outer radius of the inner channel matching the inner radius of the outer channel. The metamaterial matching layer is sealed at both ends with front and back plates, directing sound through a zig-zag path. The schematics and sound path within the metamaterial matching layer are shown in Fig. 3(c), and an exploded view of the 3D model and its components is displayed in Fig. 3(d). R_1, R_2, and R_3 are the inner radii of the three spiral channels, while $R_0 = 5$ cm is the inner radius of the impedance tube, and $L = 9$ cm is the total length of the metamaterial matching layer.

After establishing the geometric structure of the metamaterial matching layer, we plug it into our existing transmission line model using a 2×2 transfer matrix. The transfer matrix of the jth segment in the ith spiral channel is[16]

$$\mathbf{T_{ij}} = \begin{bmatrix} \cos(k_{ij}L/3) & jZ_{ij}\sin(k_{ij}L/3) \\ j\sin(k_{ij}L/3)/Z_{ij} & \cos(k_{ij}L/3) \end{bmatrix}, \tag{16}$$

where

$$k_{ij} = n_{ij}\omega/c_0, \tag{17}$$

$$Z_{ij} = z_{ij}/S_i = z_{ij}/\pi(R_{i-1}^2 - R_i^2)] \tag{18}$$

are the wavenumber and acoustic impedance inside the segment. The total transfer matrix of the metamaterial matching layer can be derived by

$$\mathbf{T} = \mathbf{T_{11}T_{12}T_{13}T_{21}T_{22}T_{23}T_{31}T_{32}T_{33}}. \tag{19}$$

In this manner, the impact of the metamaterial on the energy conversion rate (η) and sound absorption coefficient (α) is rigorously treated in our theoretical model. To optimize the performance, all geometric parameters, including the electrical load (R_L), are fine-tuned with genetic algorithm (GA).[25] The goal of the optimization process is to maximize the minimum energy conversion rate (η_{min}) within the targeted frequency range of 50–250 Hz.

In addition to transfer matrix analysis, we also validate our theoretical findings using numerical simulations performed in COMSOL. The optimized metamaterial structure is transformed into a full 3D geometry, which is then integrated into the original AEH model for updated simulation results. As a more computationally efficient alternative, we also examine the results of a 2D axial-symmetric model that considers effective refractive indices and impedances. As demonstrated in Fig. 5, both the 3D and 2D models yield comparable results.

The final step is to experimentally assess the energy harvesting capabilities of the metamaterial-enhanced AEH system inside a test rig. As depicted in Fig. 4, the entire system is housed within an impedance tube where both the sound absorption coefficient α and energy conversion coefficient η can be accurately measured using the standard two-microphone method. The audio signals p_1, p_2, and the electrical voltage on the load resistor are recorded using data acquisition devices and connected to a PC. The source loudspeaker is powered by a power amplifier that is connected to the sound card output of the PC. The spiral metamaterial matching layer in Fig. 3(d) is 3D printed using an in-house FDM machine and placed between the microphones and the receiving loudspeaker. The input pressure from the source speaker is calculated by

$$p_s = \frac{p_2}{\exp(j\omega x_2/c_0) + \Gamma(\omega)\exp(-j\omega x_2/c_0)}, \tag{20}$$

where x_1 and x_2 represent the distances between p_1 and p_2 and the inlet of the metamaterial sample, respectively. Γ is the reflection coefficient measured at the inlet of the metamaterial, and L_g is the gap between the metamaterial and the receiving loudspeaker. During the experiments, we found that while it is possible to construct the mechanical impedance of the loudspeaker cone Z_{ms} using the Theile-Small parameters provided by the manufacturer, better results were obtained by taking a preliminary measurement of the loudspeaker with an open circuit and substituting the numerical value of Z_{ms} throughout the theory and simulations.

The results from the GA-optimized AEH, as shown in Fig. 5, demonstrate an impressive energy conversion rate of 7.6%–15.1% within the frequency range of 50–228 Hz, making this AEH a major improvement compared to previous designs. This can be confirmed by the comparison with previously recorded AEHs in Fig. 7. Additionally, a sound absorption coefficient between 45% and 95% also makes it a good sound absorber in general. It is the first AEH to exceed a 100% fractional bandwidth $\Delta f/f_c$ while maintaining an $\eta > 1\%$. The AEH is particularly effective in the low-frequency portion of the absorption spectrum, where reducing noise is often the most challenging and harvesting sound energy is often the most

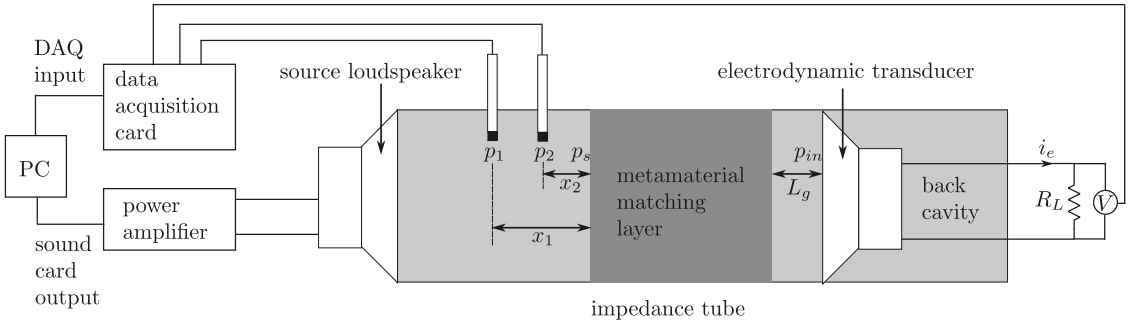

FIG. 4. Schematics of the broadband AEH experiments.

meaningful. With the total length of the folded metamaterial measuring less than 20 cm, the AEH unit is in the deep sub-wavelength regime at 50 Hz. The detailed parameters of the AEH can be found in the supplementary material. The discrepancy between the experimental results and the theoretical/numerical ones is attributed to unmodeled losses within the spiral metamaterial channels.

In previous paragraphs, we have presented a broadband acoustic energy harvester (AEH) based on metamaterial-enhanced loudspeakers. Although we have broadened the bandwidth, there is still room for improvement with regard to efficiency. An examination of Fig. 2(b) provides insight into where the input energy is being directed and how the system can be improved for higher efficiency.

Our previous assumption was that the transmission line **T** was lossless. However, this is not necessarily the case for the tortuous metamaterial structure installed in front of the loudspeaker. The fact that experimental values of $\eta(\omega)$ are generally lower than the theoretical and numerical predictions in Fig. 5 suggests that a significant amount of energy is being lost due to friction within the metamaterial channels. To minimize this loss, it may be beneficial to remove the metamaterial. The impedance Z_{ab} is mostly imaginary, as it represents the back cavity impedance, which leaves the remaining energy divided between the mechanical load Z_{as} and the electrical load Z_{ae}.

A significant portion of the incident sound is dissipated through the diaphragm vibration, i.e., $\Re[Z_{as}] = R_{ms}/S_d^2$, reducing the amount of energy available for the electrical load Z_{ae}. Once electrical current is generated in the coil, the wire resistance R_e competes with the load resistance R_L for energy. This is why we chose the 4 Ω Dayton Audio ND-91-4 over its more commonly used 8 Ω counterpart ND-91-8.

The anatomy of the transducer reveals that the center of the cone is mainly made of hard materials and that mechanical losses occur mostly in the rubber surround. To improve the energy harvesting efficiency of the AEH, we have implemented a surgical approach to reduce these mechanical losses. This involved removing the original lossy surround from the loudspeaker and replacing it with a silicone version. It is worth noting that the high Q-factor of the silicone surround produces resonant spikes in the frequency response curve when the modified transducer is used to generate sound. This is undesirable from an audio engineering perspective. As a result, most commercially available loudspeaker transducers feature fairly lossy surrounds.

The modified loudspeaker unit can be seen in Fig. 6(a), and the corresponding energy conversion rate η and sound absorption coefficient α are plotted in Fig. 6(b). The results show that the modified AEH reaches a peak energy conversion rate of 67% at 58 Hz, a threefold increase compared to the previous highest peak energy conversion rate of 22%.[10]

The aim of this section is to compare the performance of the two AEHs proposed in this paper with those mentioned in other publications. The two most crucial metrics used to evaluate the performance of AEHs are energy conversion efficiency and bandwidth. The energy conversion efficiency is defined as the proportion of output electric power in relation to the incident sound energy. Bandwidth, on the other hand, is measured in terms of the −3 dB fractional bandwidth, i.e.,

$$\Delta f/f = (f_u - f_l)/f_c. \tag{21}$$

The upper and lower frequencies, where the harvesting efficiency is half of the peak efficiency, are represented by f_u and f_l, respectively. The center frequency, f_c, is calculated as the average of f_u and f_l.

The comparison of the efficiencies and bandwidth of the AEHs in this paper with previous publications is presented in Fig. 7. Our results show that our AEHs have broken the records for both efficiency and bandwidth. Moreover, we also demonstrate that it is possible to trade bandwidth for efficiency by simply increasing the electrical load resistance of the broadband AEH.

In summary, we have designed and tested a highly effective and ultra-broadband acoustic energy harvester (AEH) using subwavelength metamaterials. Our device boasts high energy conversion efficiency, a compact design relative to the wavelength, and broad low-frequency capability. Additionally, we have demonstrated a plastic

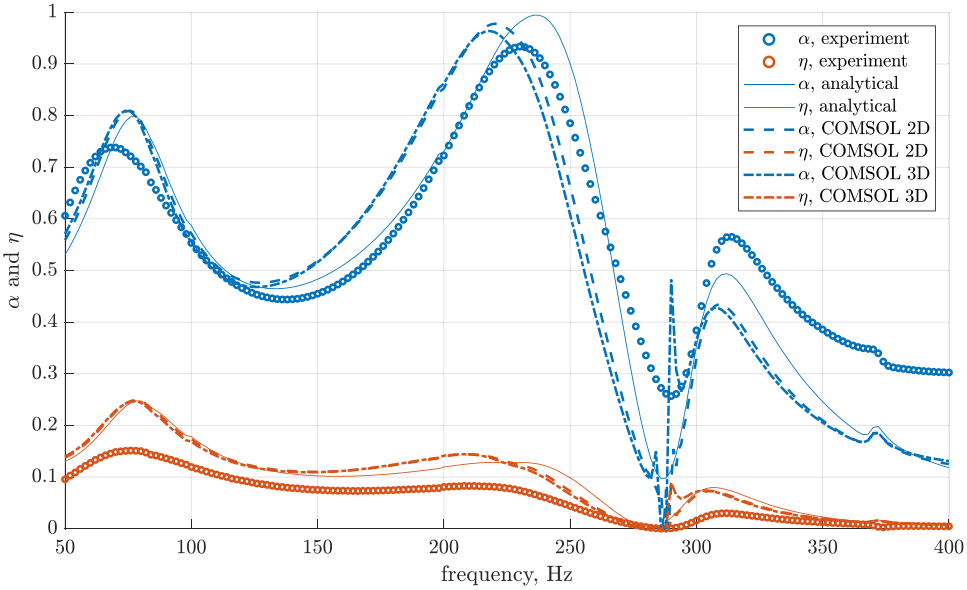

FIG. 5. Sound absorption coefficient α and energy conversion rate η of the metamaterial-enhanced broadband AEH.

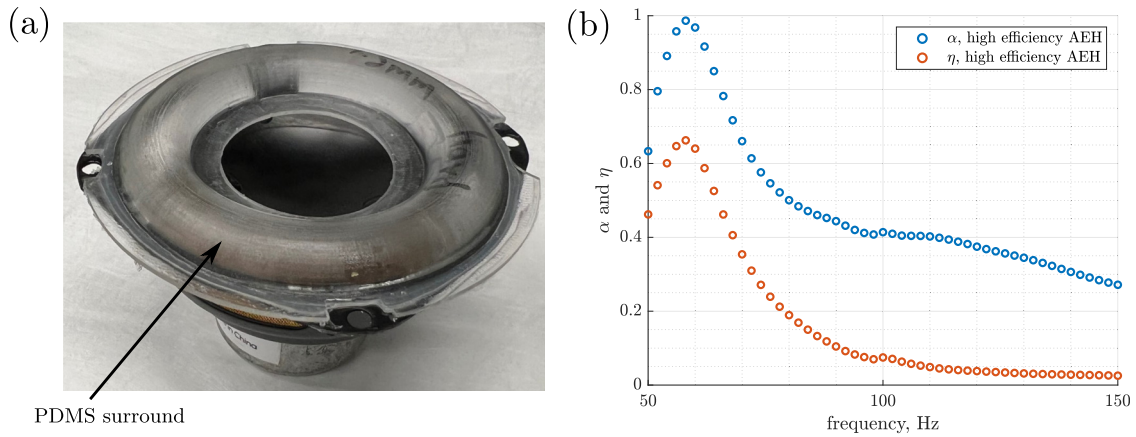

FIG. 6. (a) Picture of the high-efficiency AEH with PDMS surround. (b) Sound absorption coefficient α and energy conversion rate η of the high-efficiency AEH with PDMS surround.

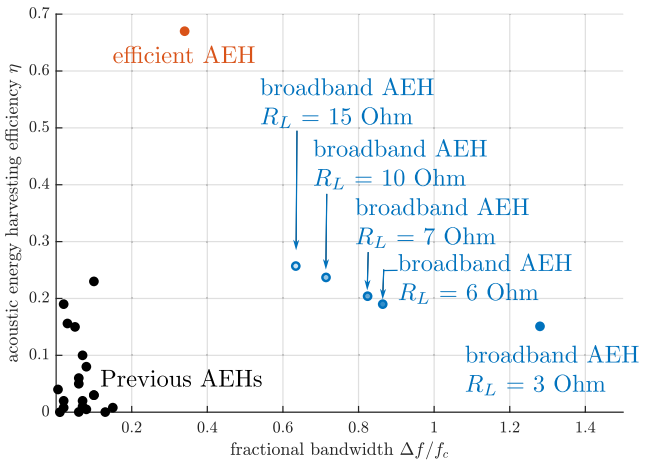

FIG. 7. Comparison of the efficiency η and fractional bandwidth Δ/f_c of AEHs.

surgery approach that further increases the peak energy conversion rate by replacing the original loudspeaker surround with a low-loss PDMS surround. The use of a commercially available loudspeaker driver makes the AEH suitable for large-scale deployment, making it a cost-effective solution for energy generation and noise reduction in various scenarios such as near factories, mass transit infrastructure, and airport runways.

See the supplementary material for the detailed efficiency/bandwidth comparison with previous AEHs and the geometrical parameters of the spiral metamaterial.

This work was supported by CMMI Grant from the National Science Foundation (Grant No. 1951106) and the Sony Research Award Program (Grant No. S168-RAP2020).

AUTHOR DECLARATIONS

Conflict of Interest

The authors have no conflicts to disclose.

Author Contributions

Xiuyuan Peng and Junfei Li contributed equally to this paper.

Xiuyuan Peng: Conceptualization (equal); Data curation (equal); Formal analysis (equal); Methodology (equal); Software (equal); Validation (equal); Visualization (equal); Writing – original draft (equal); Writing – review & editing (equal). **Junfei Li:** Conceptualization (equal); Data curation (equal); Formal analysis (equal); Methodology (equal); Software (equal); Validation (equal); Writing – review & editing (equal). **Steven A. Cummer:** Funding acquisition (lead); Investigation (lead); Project administration (lead); Resources (lead); Supervision (lead); Writing – review & editing (lead).

DATA AVAILABILITY

The data that support the findings of this study are available from the corresponding author upon reasonable request.

REFERENCES

[1]A. T. Patil and M. B. Mandale, Noise Vib. Worldwide **52**, 397 (2021).
[2]Z. Wen, W. Wang, A. Khelif, B. Djafari-Rouhani, and Y. Jin, Appl. Phys. Lett. **120**, 020501 (2022).
[3]S. K. Karan, S. Maiti, J. H. Lee, Y. K. Mishra, B. B. Khatua, and J. K. Kim, Adv. Funct. Mater. **30**, 2004446 (2020).
[4]G. Hu, L. Tang, J. Liang, C. Lan, and R. Das, Smart Mater. Struct. **30**, 085025 (2021).
[5]C. Song, J. Zhao, X. Ma, M. Zhang, W. Yuan, F. Yang, Z. Wang, X. Zhang, and Y. Pan, AIP Adv. **11**, 115002 (2021).
[6]X. Peng, Y. Wen, P. Li, A. Yang, and X. Bai, Appl. Phys. Lett. **103**, 164106 (2013).
[7]C. Song, *et al.*, "Broadband sound absorption and energy harvesting by a graded array of helmholtz resonators," in *IEEE Transactions on Dielectrics and Electrical Insulation* (IEEE, 2022), Vol. 29, pp. 777–783.
[8]N. M. Monroe and J. H. Lang, Smart Mater. Struct. **28**, 055032 (2019).
[9]A. Yang, P. Li, Y. Wen, C. Lu, X. Peng, W. He, J. Zhang, D. Wang, and F. Yang, Rev. Sci. Instrum. **85**, 066103 (2014).

[10]G. Ma, M. Yang, S. Xiao, Z. Yang, and P. Sheng, Nat. Mater. **13**, 873 (2014).
[11]F. Khan and I. Haq, Sadhana **41**, 397–405 (2016).
[12]F. U. KhanIzhar, Rev. Sci. Instrum. **87**, 025003 (2016).
[13]Z. Li, D.-Q. Yang, S.-L. Liu, S.-Y. Yu, M.-H. Lu, J. Zhu, S.-T. Zhang, M.-W. Zhu, X.-S. Guo, H.-D. Wu *et al.*, Sci. Rep. **7**, 42863 (2017).
[14]N. Cui, X. Jia, A. Lin, J. Liu, S. Bai, L. Zhang, Y. Qin, R. Yang, F. Zhou, and Y. Li, Nanoscale Adv. **1**, 4909 (2019).
[15]L. L. Beranek and T. Mellow, *Acoustics: Sound Fields and Transducers* (Academic Press, 2012).
[16]L. E. Kinsler, A. R. Frey, A. B. Coppens, and J. V. Sanders, *Fundamentals of Acoustics* (John Wiley & Sons, 2000).
[17]See https://www.comsol.com/model/lumped-loudspeaker-driver-12295 for "Lumped loudspeaker driver," (Last accessed 11 August 2023).
[18]J. Choi, I. Jung, and C.-Y. Kang, Nano energy **56**, 169 (2019).
[19]M. Yuan, Z. Cao, J. Luo, and X. Chou, Micromachines **10**, 48 (2019).
[20]Z. Chen, B. Guo, Y. Yang, and C. Cheng, Phys. B: Condens. Matter **438**, 1 (2014).
[21]G.-S. Liu, Y.-Y. Peng, M.-H. Liu, X.-Y. Zou, and J.-C. Cheng, Appl. Phys. Lett. **113**, 153503 (2018).
[22]Q. Zhang, Z. Xi, Y. Wang, L. Liu, H. Yu, H. Wang, and M. Xu, "Multi-tube helmholtz resonator based triboelectric nanogenerator for broadband acoustic energy harvesting," Front. Mater. **9**, 896953 (2022).
[23]H. Zhao, X. Xiao, P. Xu, T. Zhao, L. Song, X. Pan, J. Mi, M. Xu, and Z. L. Wang, Adv. Energy Mater. **9**, 1902824 (2019).
[24]Y. Ding, E. C. Statharas, K. Yao, and M. Hong, Appl. Phys. Lett. **110**, 241903 (2017).
[25]L. Davis, *Handbook of Genetic Algorithms* (Van Nostrand Reinhold, New York, NY, 1991).